Advances in Computational Science and Engineering
Vol. 2, No. 2, June 2024, pp. 152-173
doi:10.3934/acse.2024009

MULTI-DOMAIN MODELING AND SIMULATION OF BLOOD SOLUTES AND ELUTION IN STENTED ARTERIES

Irving Martinez[✉*1] and Alessandro Veneziani[✉2]

[1]Department of Mathematics, Aarhus University,
Ny Munkegade 118, building 1535, 328, 8000 Aarhus C, Denmark

[2]Department of Mathematics, Department of Computer Science, Emory University,
400 Dowman Dr NE, Atlanta (GA) 30322, USA

(Communicated by Annalisa Quaini)

Abstract. The introduction of Bioresorbable Stents (BRS) in angioplasty (the clinical operation to reopen an occluded coronary with intravascular procedures), originally saluted as an important innovation, was a failure for many associated adverse events. Yet, the clinical community advocates for BRS as an unmet clinical need. The reason for the failures can be associated with the special size of the bioresorbable scaffold: the absence of a metallic core calls for an increased thickness, suspected of triggering abnormal flow patterns and biological inflammations, leading to adverse events. Accurate mathematical modeling of the fluid-wall-strut interaction and the related elution of the struts can provide a breakthrough for rigorous shape optimization. Here, we model in 3D the elution process involving all three domains (fluid, wall, and struts) coexisting together. Previous studies involved only two domains. Real cases show that the stent, the lumen, and the wall are in contact with every other subdomain. The multidomain case presents nontrivial challenges. We propose a domain decomposition approach for the numerical solution using an iterative-by-subdomain method. We prove the convergence of the iterative method. We provide preliminary results in idealized yet realistic 3D geometries. Results demonstrate that the iterative method is independent of the mesh size.

1. **Introduction.** Angioplasty is a non-invasive percutaneous procedure to reopen an occluded coronary by inserting a prosthesis called "stent", deployed by balloon inflation ([8, 18, 13] and Fig. 1). The most popular prostheses are the so-called "Drug-eluting stents" (DES), where a metallic core is coated by a drug to prevent possible infections [28]. While this is a consolidated technology, *bioresorbable stents* (BRS) were introduced (see, e.g., [19, 12, 4, 18]) to avoid the significant drawback of a metallic coil located lifelong in the patient. This was supposedly an ideal solution for young patients affected by acute (as opposed to chronic) diseases. However, the number of adverse events associated with BRS led to their withdrawal from the

2020 *Mathematics Subject Classification.* Primary: 65M55; Secondary: 35Q92, 76D05.
Key words and phrases. Bioresorbable stents, multi-domain problems, domain decomposition methods.
The second author is supported by US NSF Projects DMS 2012686 (PI: Veneziani), DMS 2038118 (PI: Nagy) and the US NIH Project R01EB031101 (PI: Lindsey).
*Corresponding author: Irving Martinez.

market. A common speculation is that the abnormal thickness required by the non-metallic structure to stand the pressure during deployment may trigger anomalous flow patterns downstream the struts; these patterns, in turn, may induce inflammations with a consequent re-occlusion of the artery. This case study pinpoints the importance of more accurate and massive numerical modeling behind the design of prostheses in biomedicine. Either for a deeper understanding of the complex dynamics (ranging from mechanics to biology related to the geometry of stented arteries) or for a rigorous shape-optimization (rooted in mathematical methods), the role of numerical modeling in this field is critical. On the other hand, the biomedical community still considers BRS an unmet clinical need [19, 12, 4]. Quoting [12]: "Important lessons about strut thickness, vessel wall coverage and their influence on thrombosis induced by shear forces and the timing of degradation must be better understood before this technology can become mainstream. Before initiating large trials in humans, we need to ensure that the technology is sound and that the trial design is flawless and based on solid science."

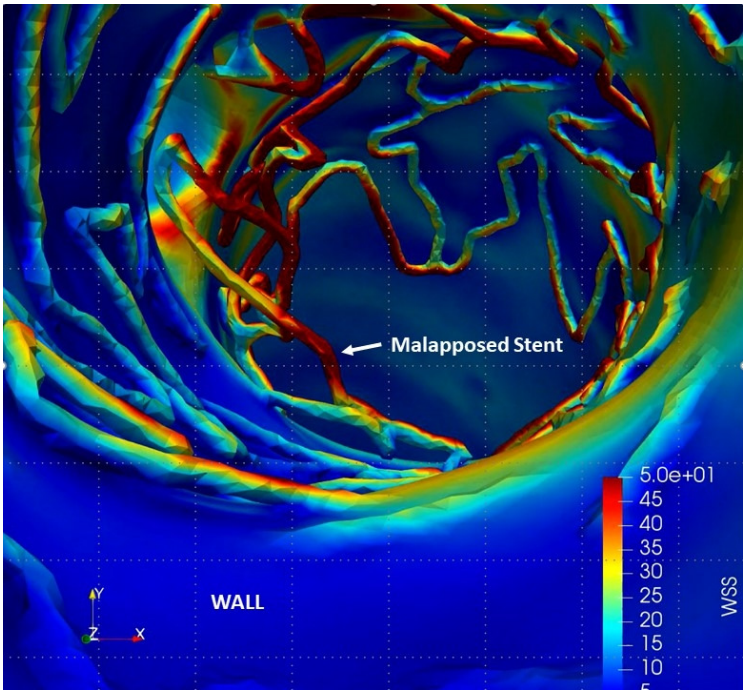

FIGURE 1. Reconstruction of a stented artery with a malapposed stent. The picture shows the occurrence of a malapposed stent, i.e., a strut that enters the lumen from the wall. In general, the struts are in contact with both the wall and the lumen at the same time [14].

Recent studies [14] demonstrated the tremendous complexity of the morphology of stented arteries. At the bottom line, we have three different domains in this problem: the lumen (L) of the coronary, the wall (W), and the struts of the stent (S). They are in contact in various ways, ranging from struts completely embedded in the wall to struts floating in the lumen as in the case of so-called "malapposed

stents" (Fig. 1). Numerical modeling of the erosion of the struts is a key factor for shape optimization and design; it must include the three domains in all the possible conformations that may happen in patients.

Modeling of the elution of DES was considered in several papers with a different complexity depending on the emphasis on the chemical elution process or on the numerical efficiency. For instance, in [7], the authors consider a complex elution model only for cases when the struts are all embedded in the wall, so the different domains are pairwise in contact. Considering the general case where the three domains are all in contact is not just a mere geometrical extension. The time scale of the elution at the interface between the wall and the struts is generally slower, as the wall has a small convective field (the motion of water in the wall is minimal); on the contrary, the interface between the lumen and the strut features a much stronger convective field (the blood velocity), consequently causing much faster erosion. When we assume the compresence of all the interfaces, the simultaneous presence of different scales may challenge the numerical solver.

In this paper, we focus specifically on a numerical method for a simplified elution model inspired by the works for generic blood solutes in [22, 23], where only two domains (lumen and wall) were present, with only one interface. Assuming that all the possible positions among the different sub-domains are possible, we provide a multi-domain, multi-interface formulation of the problem (Sect. 2). We analyze the well-posedness of the problem (Sect. 2.3). After presenting the numerical approximation, with a classical finite difference discretization in time and finite elements in space (Sect. 3), we present an iterative-by-subdomains solution method. The numerical solution of the multidomain problem is the limit of an iterative process where each physical subdomain is solved separately using the iterated interface conditions as boundary conditions. A convergence proof for the iterative-by-subdomains method is given (Sect. 4). We present several numerical results in idealized geometries and for different values of the parameters of the problem. Numerical results - quite unexpectedly - demonstrate the independence of the number of iterations of the mesh size (Sect. 5). A rigorous analysis of this circumstance is in order. As a matter of fact, while mesh-independence for two subdomains was proved in [22, 23] resorting to Steklov-Poincaré operators, the extension to three subdomains and three interfaces raises non-trivial challenges that will be addressed in a forthcoming paper (see Sect. 6).

This work is a contribution toward the construction of a numerical solver to enable an accurate modeling of the interaction between the struts and the fluid, as well as a shape-optimization analysis to identify engineering solutions for the next generation of BRS and stent in general.

1.1. **The geometrical domain.** We consider a geometry $\overline{\Omega} \subset \mathbb{R}^d, (d = 2, 3)$ composed by three sub-domains, the lumen Ω_l, the wall Ω_w, and the strut Ω_s, belonging to $\mathbb{R}^d$ and any two of which share a boundary interface (See Figure 2). The boundary $\partial\Omega$ of $\overline{\Omega}$ is divided into proximal sections $\partial\Omega_{in} = \Gamma_{l,in} \cup \Gamma_{w,in}$, distal sections $\partial\Omega_{out} = \Gamma_{l,out} \cup \Gamma_{w,out}$, and the external longitudinal boundary $\Gamma_{w,ext}$.

1. The domain Ω_w is the outermost shell of $\overline{\Omega}$ such that its outer surface $\Gamma_{w,ext}$ along the longitudinal axis of $\overline{\Omega}$ equals the outer surface of $\overline{\Omega}$. Its closure intersects intermittently both Ω_l and Ω_s at $(d-1)$-manifolds Γ_{lw} and Γ_{sw}, respectively. In other words, these intersections are such that $\Gamma_{lw} = \overline{\Omega_w} \cap \overline{\Omega_l}$, $\Gamma_{ls} = \overline{\Omega_l} \cap \overline{\Omega_s}$ and $\Gamma_{sw} = \overline{\Omega_w} \cap \overline{\Omega_s}$. The solute on upstream portions of the

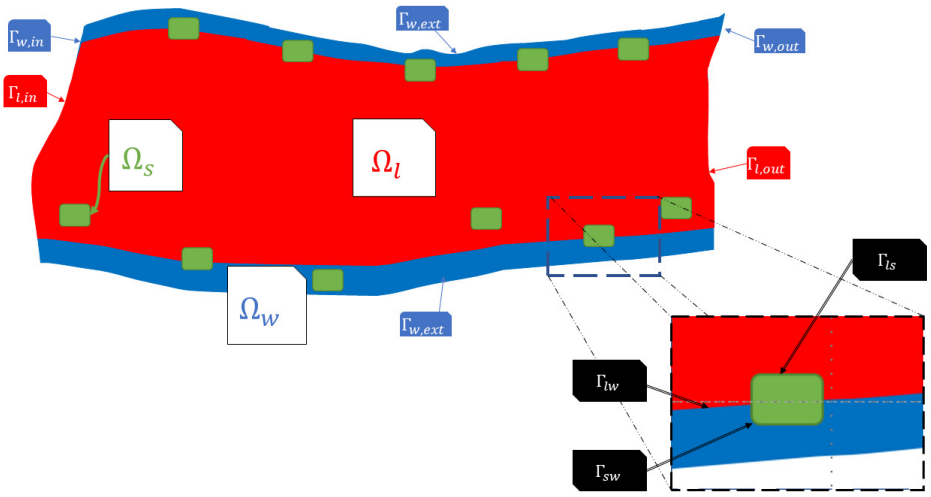

FIGURE 2. Diagram of the geometry of interest. We focus on the case where the three domains (lumen Ω_l, wall Ω_w, and struts Ω_s) are all in contact simultaneously, like in the zoomed square.

stent will enter through the incoming boundary $\Gamma_{w,in}$ and exit through the outgoing boundary $\Gamma_{w,out}$.

2. Ω_l is the lumen of the artery, surrounded by the wall Ω_w with the interface Γ_{lw} and interfacing the stent at Γ_{ls}. Blood and solute enter the lumen from $\Gamma_{l,in}$ and leave through $\Gamma_{l,out}$. In this domain, the blood velocity is responsible for the convection of the drug dynamics.
3. The third subdomain Ω_s is the strut of the stent. In general, the stent is a continuous net-like structure that presents some portion embedded in the wall, some in the lumen, and some parts interfacing with both the other domains [5]. We will focus on this latter case, assuming that the three domains have all non-empty interfaces (see Figure 2, in particular the zoomed part). In Ω_s, no fluid flows.

In general, the material of the stent can be metallic (bare metal stents) metallic and polymeric (drug-eluting stents) or purely polymeric (bioresorbable stents). Bare metal stents are obsolete, while the other two types feature erosion on a time scale that is generally much larger than the one of the heart-beat. In this paper, we focus on the heart-beat scale (order of seconds), so we assume that the geometry of the strut is constant in time. For simplicity, we also do not include the mechanical interaction between the wall and the blood.

We do not specifically focus on the case when the strut is surrounded only by either the wall or the lumen, as these cases are locally already included in the available literature [7]. In our setting we postulate

$$\partial\Omega_s = \Gamma_{ls} \cup \Gamma_{sw}, \ \text{meas}(\Gamma_{ls}) > 0, \ \text{meas}(\Gamma_{sw}) > 0.$$

We also do not consider the case when a portion of the boundary of the struts is on the external boundary of the domain, as this case is technically simpler (the Poincaré inequality applies to the strut domain). The case we consider is the one

zoomed in Fig. 2, and it is the most complicated one from both the mathematical and numerical point of view.

1.2. **Functional spaces and notation.** Using a standard notation, we denote by $L^2(\Omega)$ the space of square-summable functions in Ω, and $H^k(\Omega)$ the space with square-summable derivatives up to the order k; $H^1_\Gamma(\Omega)$ denotes the space of functions in $H^1(\Omega)$ vanishing on $\Gamma \subset \partial\Omega$. For the sake of notation, we will denote $V_{D,j} \equiv H^1_{\Gamma_{j,in}}(\Omega_j)$ for $j = l, w$ (where D stands for Dirichlet, as we postulate Dirichlet conditions at the inflow). The boldface notation $\mathbf{V}_{D,l}$ is used for the vector functions in $[H^1(\Omega_l)]^d$ vanishing on the portion of the boundary where Dirichlet conditions are prescribed (in the case of blood: $\Gamma_{l,in} \cup \Gamma_{ls} \cup \Gamma_{lw}$). Hereafter, we also denote by V_s the space $H^1(\Omega_s)$. We also denote by $(\cdot,\cdot)_i$ the $L^2(\Omega_i)$ scalar product for $i = l, s, w$. The special notation Q is used for the space $L^2(\Omega_l)$. The notation $\|\cdot\|_{1,i}$ will be used for the norm in the space $H^1(\Omega_i)$.

Then, $L^2(H^k)$ will be the shorthand notation for $L^2(0,T;H^k(\Omega))$, functions whose $H^k(\Omega)$ norm is a $L^2(0,T)$ function of time. Similar definition for $L^\infty(L^2)$, functions whose $L^2(\Omega)$ norm is bounded in time.

If Σ denotes a manifold in $\bar{\Omega}$ such that $\Sigma \cap \Gamma \neq \emptyset$, the trace of functions in $H^1_\Gamma(\Omega)$ on Σ belongs to a subspace of $H^{1/2}(\Sigma)$ that we will denote by Λ. We will use subscripts to indicate which portion of the interface the space refers to (e.g., Λ_{ls} refers to the traces on Γ_{ls}). For the interfaces, the indexes will follow a lexicographic order (ls, lw, sw).

For a generic positive bounded function $\zeta_{ij} \in L^\infty(\Gamma_{ij})$, and two functions $f, g \in \Lambda_{ij}$ $(i, j = l, s, w$ with $i \neq j)$, we denote

$$(f,g)_{ij} \equiv \int_{\Gamma_{ij}} \zeta_{ij} f g d\Gamma, \|f\|^2_{ij} \equiv (f,f)_{ij}$$

Finally, we let $\gamma : H^1(\Omega) \to H^{1/2}(\Sigma)$ be the surjective and continuous trace operator [2]; on the other hand, the existence of a lifting map $\mathcal{L} : H^{1/2}(\Sigma) \to H^1(\Omega)$ such that it is injective, linear, and continuous and that for all $\lambda \in H^{1/2}(\Sigma)$ we have $\lambda = \gamma\mathcal{L}\lambda$ can be proven [1].

2. Problem formulation.

2.1. **Blood equations.** We consider blood as a Newtonian fluid with constant viscosity ν, described by the incompressible unsteady Navier-Stokes Equations [24]. For $\mathbf{x} \in \Omega_l$ and $t > 0$ we let $\boldsymbol{u}(t,\mathbf{x}) \in \mathbb{R}^d$ be the velocity of blood and $P(t,\mathbf{x})$ its pressure that solve the equations:

$$\begin{cases} \rho\dfrac{\partial \boldsymbol{u}}{\partial t} + \rho(\boldsymbol{u}\cdot\nabla)\boldsymbol{u} - \nu\Delta\boldsymbol{u} + \nabla P = \mathbf{f} \quad x \in \Omega_l, \qquad t > 0, \\ \nabla\cdot\boldsymbol{u} = 0 \quad \mathbf{x} \in \Omega_l, \qquad t > 0, \\ \boldsymbol{u} = \mathbf{b} \quad \text{on} \quad \Gamma_{l,in}, \quad t > 0, \\ \boldsymbol{u} = \mathbf{0} \quad \text{on} \quad \Gamma_{lw} \cup \Gamma_{ls}, t > 0, \\ P\mathbf{n} - \nu\nabla\boldsymbol{u}\cdot\mathbf{n} = P_{ext}\mathbf{n} \quad \text{on} \quad \Gamma_{l,out} \qquad t > 0, \\ \boldsymbol{u}(0,\mathbf{x}) = \boldsymbol{u}_0(\mathbf{x}) \quad \text{with} \quad \nabla\cdot\boldsymbol{u}_0 = 0, \quad \mathbf{x} \in \Omega_l. \end{cases} \tag{1}$$

Here $\mathbf{f}$ is a local source function, such as gravity, $\mathbf{b}$ is the inflow blood velocity function, $\boldsymbol{u}_0$ is the initial blood velocity in Ω_l at time $t = 0$, P_{ext} (that we set to 0) is the external pressure, and $\mathbf{n}$ is the outward normal unit vector to the boundaries

of Ω_l. We assume the initial conditions $\boldsymbol{u}_0$ to be compatible with the boundary conditions at $t = 0$.

For the sake of simplicity, in the analysis, we assume the Dirichlet boundary conditions to be homogeneous.

2.1.1. *Weak formulation of the blood problem.* Using standard arguments (see, e.g., [27, 10]), we obtain the weak formulation for the Navier-Stokes equations by multiplying the momentum equation by a test function $\boldsymbol{v} \in \mathbf{V}_{D,l}$ and the mass conservation by a test function $q \in Q$. After standard applications of the Green formula, we obtain the following problem.

Problem 1. *Given* $\boldsymbol{u}_0 \in (L^2(\Omega_l))^d$ *with* $\nabla \cdot \boldsymbol{u}_0 = 0$ *and* $f \in L^2((L^2(\Omega_l))^d)$, *find* $\boldsymbol{u} \in L^2(\mathbf{V}_{D,l}) \cap L^\infty((L^2(\Omega_l))^d)$ *and* $P \in L^2(L^2(\Omega_l))$ *such that for all* $t > 0$

$$\begin{cases} \left(\dfrac{\partial \boldsymbol{u}}{\partial t}, \boldsymbol{v}\right) + \nu(\nabla \boldsymbol{u}, \nabla \boldsymbol{v}) + ((\boldsymbol{u} \cdot \nabla)\boldsymbol{u}, \boldsymbol{v}) - (\nabla \cdot \boldsymbol{v}, P) = (\mathbf{f}, \boldsymbol{v}) \quad \forall \boldsymbol{v} \in \mathbf{V}_{D,l}, \\ (\nabla \cdot \boldsymbol{u}, q) = 0 \quad \forall q \in Q, \end{cases} \tag{2}$$

with $\boldsymbol{u}(\mathbf{x}, 0) = \boldsymbol{u}_0$ *for* $t = 0, \mathbf{x} \in \Omega_l$.

As well known, the well-posedness of this problem is still the subject of active research. We refer to the abundant literature for a recap [15, 16, 17, 11, 27, 26, 10, 9]. In what follows, we will simply assume that the velocity and pressure fields exist, are unique, and are regular enough for the following analysis.

2.2. **Concentration equations.** The solute is released by the stent into Ω_w and Ω_l. To describe elution, we introduce the concentration fields C_l, C_w, C_s; we assume that C_l is subject to an advection-diffusion process, where the convection is given by $\boldsymbol{u}$. In the wall, we assume that the drug concentration is subject to diffusion only.

Consequently, for $t > 0$, the equations and the boundary conditions for the concentrations $C_i(t, \mathbf{x})$ $(i = l, w, s)$ that we consider read as follows [22, 23].

$$\begin{aligned} &\frac{\partial C_l}{\partial t} - \mu_l \Delta C_l + \boldsymbol{u} \cdot \nabla C_l = s_l \quad \text{in} \quad \Omega_l, \quad t > 0, \\ &C_l = C_{l,in} \quad \text{on} \quad \Gamma_{l,in}, \quad \mu_l \frac{\partial C_l}{\partial \boldsymbol{n}_l} = 0 \quad \text{on} \quad \Gamma_{l,out}, \end{aligned} \tag{3}$$

$$\begin{aligned} &\frac{\partial C_w}{\partial t} - \mu_w \Delta C_w = s_w \quad \text{in} \quad \Omega_w, \quad t > 0, \\ &C_w = C_{w,in} \quad \text{on} \quad \Gamma_{w,in}, \quad \mu_w \frac{\partial C_w}{\partial \boldsymbol{n}_w} = 0 \quad \text{on} \quad \Gamma_{w,out}, \end{aligned} \tag{4}$$

$$\frac{\partial C_s}{\partial t} - \mu_s \Delta C_s = s_s \quad \text{in} \quad \Omega_s, \quad t > 0, \tag{5}$$

Here, for $i = l, w, s$, the s_i represent source (forcing) functions, μ_i are the positive diffusivities in their respective domains, $\boldsymbol{n}_i$ are the outward unit vectors. Furthermore, the following interface conditions hold as well [22]. Let ζ_{ls}, ζ_{lw}, and ζ_{sw} be three positive bounded functions defined on the interfaces denoted by their subscripts.

$$\begin{cases} \mu_l \dfrac{\partial C_l}{\partial \boldsymbol{n}_l} + \zeta_{lw}(C_l - C_w) = 0, \\ \mu_w \dfrac{\partial C_w}{\partial \boldsymbol{n}_w} + \mu_l \dfrac{\partial C_l}{\partial \boldsymbol{n}_l} = 0, \end{cases} \quad \text{on} \quad \Gamma_{lw}; \tag{6}$$

$$\begin{cases} \mu_s \dfrac{\partial C_s}{\partial \boldsymbol{n}_s} + \zeta_{ls}(C_s - C_l) = 0, \\ \mu_l \dfrac{\partial C_l}{\partial \boldsymbol{n}_l} + \mu_s \dfrac{\partial C_s}{\partial \boldsymbol{n}_s} = 0, \end{cases} \quad \text{on} \quad \Gamma_{ls}; \tag{7}$$

$$\begin{cases} \mu_w \dfrac{\partial C_w}{\partial \boldsymbol{n}_w} + \zeta_{sw}(C_w - C_s) = 0, \\ \mu_s \dfrac{\partial C_s}{\partial \boldsymbol{n}_s} + \mu_w \dfrac{\partial C_w}{\partial \boldsymbol{n}_w} = 0, \end{cases} \quad \text{on} \quad \Gamma_{sw}. \tag{8}$$

Notice that (6), (7), and (8) give respectively

$$\mu_w \frac{\partial C_w}{\partial \boldsymbol{n}_w} + \zeta_{lw}(C_w - C_l) = 0, \quad \text{on} \quad \Gamma_{lw}, \tag{9}$$

$$\mu_l \frac{\partial C_l}{\partial \boldsymbol{n}_l} + \zeta_{ls}(C_l - C_s) = 0, \quad \text{on} \quad \Gamma_{ls}, \tag{10}$$

$$\mu_s \frac{\partial C_s}{\partial \boldsymbol{n}_s} + \zeta_{sw}(C_s - C_w) = 0, \quad \text{on} \quad \Gamma_{sw}, \tag{11}$$

Finally, we prescribe the initial conditions

$$C_l(\mathbf{x}, 0) = C_{l0}(\mathbf{x}), \quad \mathbf{x} \in \Omega_l, \quad C_w(\mathbf{x}, 0) = C_{w0}(\mathbf{x}), \quad \mathbf{x} \in \Omega_w,$$
$$C_s(\mathbf{x}, 0) = C_{s0}(\mathbf{x}), \quad \mathbf{x} \in \Omega_s.$$

2.2.1. *Weak formulation of the concentration problem.* With a standard procedure, for $v_l \in L^2(V_{D,l})$, $v_w \in L^2(V_{D,w})$, $v_s \in L^2(V_s)$ we introduce the bilinear forms

$$\begin{cases} a_l(C_l, v_l) \equiv \mu_l \int_{\Omega_l} \nabla C_l \cdot \nabla v_l d\omega + \int_{\Omega_l} (\boldsymbol{u} \cdot \nabla C_l) v_l d\omega \\ a_w(C_w, v_w) \equiv \mu_w \int_{\Omega_w} \nabla C_w \cdot \nabla v_w d\omega \\ a_s(C_s, v_s) \equiv \mu_s \int_{\Omega_s} \nabla C_s \cdot \nabla v_s d\omega \end{cases} \tag{12}$$

Notice that the bilinear forms a_l, a_w, and a_s are continuous and, if $\boldsymbol{u} \cdot \boldsymbol{n}_l > 0$ on $\Gamma_{l,out}$, a_w and a_l are coercive with coercivity constants α_l, α_w; also, a_w and a_s are symmetric, and a_s is weakly coercive, i.e. there exist two positive constants α_s and σ_s s.t. $a_s(C_s, C_s) + \sigma_s \int_{\Omega_s} C_s^2 d\omega \geq \alpha_s \|C_s\|^2_{V_s}$.

With this notation, the concentration problem reads as follows.

Problem 2. *Given the initial conditions*

$$C_l(0, \mathbf{x}) = C_l^0(\mathbf{x}) \in V_{D,l}, \; C_w(0, \mathbf{x}) = C_w^0(\mathbf{x}) \in V_{D,w}, \; C_s(0, \mathbf{x}) = C_s^0(\mathbf{x}) \in V_s$$

and given $s_j \in L^2(L^2(\Omega_j))$ with $j = l, s, w$, and the positive functions $\zeta_{lw} \in L^\infty(\Gamma_{lw})$, $\zeta_{sw} \in L^\infty(\Gamma_{sw})$, and $\zeta_{ls} \in L^\infty(\Gamma_{ls})$, find $C_l \in L^2(V_{D,l})$, $C_w \in L^2(V_{D,w})$, and $C_s \in L^2(V_s)$ such that for all $\phi_l \in V_{D,l}$, $\phi_w \in V_{D,w}$, and $\phi_s \in V_s$ the following system holds

$$\begin{cases} \left(\dfrac{\partial C_l}{\partial t}, \phi_l\right) + a_l(C_l, \phi_l) + (C_l - C_w, \phi_l)_{lw} + (C_l - C_s, \phi_s)_{ls} = (s_l, \phi_l)_l, \\ \left(\dfrac{\partial C_w}{\partial t}, \phi_w\right) + a_w(C_w, \phi_w) + (C_w - C_s, \phi_w)_{sw} + (C_w - C_l, \phi_w)_{lw} = (s_w, \phi_w)_w, \\ \left(\dfrac{\partial C_s}{\partial t}, \phi_s\right) + a_s(C_s, \phi_s) + (C_s - C_l, \phi_s)_{ls} + (C_s - C_w, \phi_s)_{sw} = (s_s, \phi_s)_s, \end{cases}$$

2.3. **Well-posedness analysis.**

Theorem 2.1. *For $\boldsymbol{u} \in L^\infty(L^2(\Omega_l)) \cap L^2(V_{D,l})$ with $\boldsymbol{u} \cdot \boldsymbol{n}_l > 0$ on $\Gamma_{l,out}$, Problem 2 admits a unique solution that depends continuously on the data.*

Proof. Adding up the equations in Problem 2 and rearranging the terms

$$(C_l - C_w, \phi_l)_{lw} + (C_w - C_l, \phi_w)_{lw} = (C_l - C_w, \phi_l - \phi_w)_{lw}$$
$$(C_w - C_s, \phi_w)_{sw} + (C_s - C_w, \phi_s)_{sw} = (C_w - C_s, \phi_w - \phi_s)_{sw}$$
$$(C_s - C_l, \phi_s)_{ls} + (C_l - C_s, \phi_l)_{ls} = (C_s - C_l, \phi_s - \phi_l)_{ls}$$

we obtain the expression

$$\left(\frac{\partial \mathbf{C}}{\partial t}, \mathbf{\Phi}\right) + \mathcal{A}(\mathbf{C}, \mathbf{\Phi}) = (\mathbf{S}, \mathbf{\Phi}), \tag{13}$$

where

$$\mathbf{C} = [C_l, C_w, C_l]^T, \quad \mathbf{\Phi} = [\phi_l, \phi_w, \phi_s]^T, \quad \mathbf{S} = [s_l, s_w, s_s]^T,$$
$$\mathcal{A}(\mathbf{C}, \mathbf{\Phi}) = a_l(C_l, \phi_l) + a_w(C_w, \phi_w) + a_s(C_s, \phi_s) +$$
$$(C_l - C_w, \phi_l - \phi_w)_{lw} + (C_w - C_s, \phi_w - \phi_s)_{sw} + (C_s - C_l, \phi_s - \phi_l)_{ls}$$
$$(\mathbf{S}, \mathbf{\Phi}) = (s_l, \phi_l)_l + (s_w, \phi_w)_w + (s_s, \phi_s)_s .$$

Now, the bilinear form $\mathcal{A}(\cdot, \cdot)$ is continuous and weakly coercive. Since the right-hand side of (13) is a linear and continuous functional in $V_{D,l} \times V_{D,w} \times V_s$, we can establish the well-posedness of Problem 2 through the Faedo-Galerkin method (see e.g. [21]). □

Remark 2.2. In our problem set, we are excluding that the struts Ω_s have boundaries other than the interfaces with Ω_l and Ω_w so that a_s is weakly coercive since the Poincaré inequality does not apply. Admitting that the strut may have an external portion of the boundary, where homogeneous Dirichlet conditions apply, actually simplifies our analysis since a_s is then coercive.

3. **Numerical approximation.**

3.1. **Time semi-discretization.** We consider the time discretization of Problem 2. We let the time interval $[0, T]$ be divided into N subintervals of uniform length $\Delta t > 0$ such that $t^n = n\Delta t$ for $n = 0, 1, ..., N$. For simplicity, we consider the case of a backward Euler discretization, the extension to more accurate time discretization schemes (e.g. multisteps) being basically a technical improvement for which the subsequent analysis applies.

Let us set $\chi = \dfrac{1}{\Delta t}$ and the following definitions:

$$\hat{a}_l(C_l, v_l) = \chi(C_l, v_l)_l + a_l(C_l, v_l) \quad \forall v_l \in V_{D,l} \tag{14}$$

$$\hat{a}_w(C_w, v_w) = \chi(C_w, v_w)_w + a_w(C_w, v_w) \quad \forall v_w \in V_{D,w} \tag{15}$$

$$\hat{a}_s(C_s, v_s) = \chi(C_s, v_s)_s + a_s(C_s, v_s) \quad \forall v_s \in V_s \tag{16}$$

Observe that each of these forms is bilinear and coercive, with $\hat{a}_w$ and $\hat{a}_s$ being additionally symmetric. We denote by $\hat{\alpha}_l, \hat{\alpha}_s$ and $\hat{\alpha}_w$ the corresponding coercivity constants.

Problem 3. *Given C_l^0, C_w^0, and C_s^0 for every $n = 0, 1, ..., N-1$ find*

$$C_l^{n+1} \in V_{D,l}, \quad C_w^{n+1} \in V_{D,w}, \quad C_s^{n+1} \in V_s$$

such that for all $\phi_l \in V_{D,l}$, $\phi_w \in V_{D,w}$, *and* $\phi_s \in V_s$, *solve*

$$\begin{aligned}
\hat{a}_l(C_l^{n+1},\phi_l) + (C_l^{n+1},\phi_l)_{lw} + (C_l^{n+1},\phi_l)_{ls} \\
-(C_w^{n+1},\phi_l)_{lw} - (C_s^{n+1},\phi_l)_{ls} = (f_l^{n+1},\phi_l)_l \\
\hat{a}_w(C_w^{n+1},\phi_w) + (C_w^{n+1},\phi_w)_{sw} + (C_w^{n+1},\phi_w)_{lw} \\
-(C_s^{n+1},\phi_w)_{sw} - (C_l^{n+1},\phi_w)_{lw} = (f_w^{n+1},\phi_w)_w \\
\hat{a}_s(C_s^{n+1},\phi_s) + (C_s^{n+1},\phi_s)_{ls} + (C_s^{n+1},\phi_s)_{sw} \\
-(C_l^{n+1},\phi_s)_{ls} - (C_w^{n+1},\phi_s)_{sw} = (f_s^{n+1},\phi_s)_s,
\end{aligned} \tag{17}$$

where $s_l^{n+1} = s_l(t^{n+1})$, $s_w^{n+1} = s_w(t^{n+1})$, $s_s^{n+1} = s_s(t^{n+1})$ *and* $f_i^{n+1} \equiv s_i^{n+1} + \chi C_i^n$ *for* $i = i, s, w$.

Proposition 3.1. *At each time step, Problem 3 is well-posed.*

Proof. This follows from the fact that each bilinear form $\hat{a}_i$ is coercive. Summing up the three equations, we have

$$\hat{\mathcal{A}}(\mathbf{C}^{n+1},\mathbf{\Phi}) = (\mathbf{F}^{n+1},\mathbf{\Phi}), \tag{18}$$

where (we omit the time index for easiness of notation)

$$\begin{aligned}
&\hat{\mathcal{A}}(\mathbf{C},\mathbf{\Phi}) = \hat{a}_l(C_l,\phi_l) + \hat{a}_w(C_w,\phi_w) + \hat{a}_s(C_s,\phi_s) + \\
&(C_l - C_w, \phi_l - \phi_w)_{lw} + (C_w - C_s, \phi_w - \phi_s)_{sw} + (C_s - C_l, \phi_s - \phi_l)_{ls}
\end{aligned}$$

and

$$\mathbf{F} = [f_l, f_w, f_s]^T, \quad (\mathbf{F},\mathbf{\Phi}) = (f_l,\phi_l)_l + (f_w,\phi_w)_w + (f_s,\phi_s)_s\,.$$

The Lax-Milgram lemma promptly applies to (18). □

3.2. **Space discretization.** We complete the discretization of the problem in space with the finite element method. To this aim, we introduce a *conformal* reticulation of the domains $\Omega_l, \Omega_w, \Omega_s$, and the finite-dimensional subspaces $V_{h,l} \subset V_{D,l}$, $V_{h,w} \subset V_{D,w}$, $V_{h,s} \subset V_s$ of piecewise polynomial functions. The weak formulation of the discrete problem reads:

Problem 4. *Given* $C_{l,h}^0 \in V_{h,l}$, $C_{w,h}^0 \in V_{h,w}$, *and* $C_s^0 \in V_{h,s}$ *for every* $n = 0, 1, ..., N-1$ *find*

$$C_{l,h}^{n+1} \in V_{h,l}, \quad C_{w,h}^{n+1} \in V_{h,w}, \quad C_{s,h}^{n+1} \in V_{h,s}$$

such that for all $\phi_{l,h} \in V_{h,l}$, $\phi_{w,h} \in V_{h,w}$, *and* $\phi_{s,h} \in V_{h,s}$, *solve*

$$\begin{aligned}
\hat{a}_l(C_{l,h}^{n+1},\phi_{l,h}) + (C_{l,h}^{n+1},\phi_{l,h})_{lw} + (C_{l,h}^{n+1},\phi_{l,h})_{ls} \\
-(C_{w,h}^{n+1},\phi_{l,h})_{lw} - (C_s^{n+1},\phi_{l,h})_{ls} = (f_l^{n+1},\phi_{l,h})_l \\
\hat{a}_w(C_{w,h}^{n+1},\phi_{w,h}) + (C_{w,h}^{n+1},\phi_{w,h})_{sw} + (C_{w,h}^{n+1},\phi_{w,h})_{lw} \\
-(C_s^{n+1},\phi_{w,h})_{sw} - (C_{l,h}^{n+1},\phi_{w,h})_{lw} = (f_w^{n+1},\phi_{w,h})_w \\
\hat{a}_s(C_{s,h}^{n+1},\phi_{s,h}) + (C_{s,h}^{n+1},\phi_{s,h})_{ls} + (C_{s,h}^{n+1},\phi_s)_{sw} \\
-(C_{l,h}^{n+1},\phi_{s,h})_{ls} - (C_{w,h}^{n+1},\phi_{s,h})_{sw} = (f_s^{n+1},\phi_{s,h})_s.
\end{aligned} \tag{19}$$

With similar arguments to the ones used in the proof of Proposition 3.1, the previous problem can be proved to be well-posed.

4. **Iterative-by-subdomain solution of the problem.** To solve our problem avoiding the computational burden induced by the different dynamics and coefficients in the different subdomains, we perform a method based on the iterative solution of the following problems. As in the previous Sections, for the sake of readability, we do not explicitly specify the boundary conditions on the input/output sections. Also, for the sake of notation, the time index $n+1$ is understood, and the index k refers to the iterations by subdomains.

Let's assume that the initial guesses $C_l^{(0)}$, $C_w^{(0)}$ and $C_s^{(0)}$ are given (they may coincide with the converged value at the previous time step).

1. Lumen problem: Solve

$$\begin{aligned}
&\chi C_l^{(k+1)} - \mu_l \Delta C_l^{(k+1)} + \boldsymbol{u}\cdot\nabla C_l^{(k+1)} = f_l && \text{in } \Omega_l\\
&\mu_l \frac{\partial C_l^{(k+1)}}{\partial \boldsymbol{n}_l} + \zeta_{ls}(C_l^{(k+1)} - C_s^{(k)}) = 0 && \text{on } \Gamma_{ls}\\
&\mu_l \frac{\partial C_l^{(k+1)}}{\partial \boldsymbol{n}_l} + \zeta_{lw}(C_l^{(k+1)} - C_w^{(k)}) = 0 && \text{on } \Gamma_{lw}
\end{aligned}$$

   In weak terms: find $C_l^{(k+1)} \in V_l$ s.t.

$$\hat{a}_l(C_l^{(k+1)}, \phi_l) + \left(C_l^{(k+1)} - C_s^{(k)}, \phi_l\right)_{ls} + \left(C_l^{(k+1)} - C_w^{(k)}, \phi_l\right)_{lw} = (f_l, \phi_l)_l \qquad (20)$$

   for all $\phi_l \in V_l$.
2. Wall problem: Solve

$$\begin{aligned}
&\chi C_w^{(k+1)} - \mu_w \Delta C_w^{(k+1)} = f_w && \text{in } \Omega_w\\
&\mu_w \frac{\partial C_w^{(k+1)}}{\partial \boldsymbol{n}_w} + \zeta_{lw}(C_w^{(k+1)} - C_l^{(k+1)}) = 0 && \text{on } \Gamma_{lw}\\
&\mu_w \frac{\partial C_w^{(k+1)}}{\partial \boldsymbol{n}_w} + \zeta_{sw}(C_w^{(k+1)} - C_s^{(k)}) = 0 && \text{on } \Gamma_{sw}
\end{aligned}$$

   In weak terms: find $C_w^{(k+1)} \in V_w$ s.t.

$$\hat{a}_w(C_w^{(k+1)}, \phi_w) + \left(C_w^{(k+1)} - C_l^{(k+1)}, \phi_w\right)_{lw} + \left(C_w^{(k+1)} - C_s^{(k)}, \phi_w\right)_{sw} = (f_w, \phi_w)_w \qquad (21)$$

   for all $\phi_w \in V_w$.
3. Strut problem: Solve

$$\begin{aligned}
&\chi C_s^{(k+1)} - \mu_s \Delta C_s^{(k+1)} = f_s && \text{in } \Omega_s\\
&\mu_s \frac{\partial C_s^{(k+1)}}{\partial \boldsymbol{n}_s} + \zeta_{ls}(C_s^{(k+1)} - C_l^{(k+1)}) = 0 && \text{on } \Gamma_{ls}\\
&\mu_s \frac{\partial C_s^{(k+1)}}{\partial \boldsymbol{n}_w} + \zeta_{sw}(C_s^{(k+1)} - C_w^{(k+1)}) = 0 && \text{on } \Gamma_{sw}
\end{aligned}$$

   In weak terms: find $C_s^{(k+1)} \in V_s$ s.t.

$$\hat{a}_s(C_s^{(k+1)}, \phi_s) + \left(C_s^{(k+1)} - C_l^{(k+1)}, \phi_s\right)_{ls} + \left(C_s^{(k+1)} - C_w^{(k+1)}, \phi_s\right)_{sw} = (f_s, \phi_s)_s \qquad (22)$$

   for all $\phi_s \in V_s$.
4. Relaxation: Set

$$C_{i,rel}^{(k+1)} = \omega_i C_i^{(k+1)} + (1-\omega_i) C_i^{(k)}, i = l, w, s$$

where ω_i are real numbers generally in the interval $(0,1]$. The unrelaxed version corresponds to the case $\omega_i = 1$.

Finally, for the sake of the notation, we reset

$$C_i^{(k+1)} = C_{i,rel}^{(k+1)}.$$

Remark 4.1. In the sequence of problems we solve (lumen-wall-strut), we start from the lumen because we first solve the Navier-Stokes equations to compute the convective field there. It seems reasonable to use this convective field immediately. For the other problems in the sequence there is no specific reason to choose one or the other. It is promptly written a scheme solving the sequence lumen-strut-wall problems. From the convergence point of view, the two methods are equivalent.

4.1. **Convergence of the iterative-by-subdomain method.** For simplicity, we consider the unrelaxed case $\omega_i = 1$ (for $i = l, w, s$).

Let us introduce the error functions

$$e_i^{(k)} \equiv C_i^{(k)} - C_i, \qquad i = l, w, s \tag{23}$$

and consider the error equations we obtain when subtracting (20,21,22) to (17):

$$\begin{cases} \hat{a}_l(e_l^{(k+1)}, \phi_l) + \left(e_l^{(k+1)} - e_s^{(k)}, \phi_l\right)_{ls} + \left(e_l^{(k+1)} - e_w^{(k)}, \phi_l\right)_{lw} = 0 \\ \hat{a}_w(e_w^{(k+1)}, \phi_w) + \left(e_w^{(k+1)} - e_l^{(k+1)}, \phi_w\right)_{lw} + \left(e_w^{(k+1)} - e_s^{(k)}, \phi_w\right)_{sw} = 0 \\ \hat{a}_s(e_s^{(k+1)}, \phi_s) + \left(e_s^{(k+1)} - e_l^{(k+1)}, \phi_s\right)_{ls} + \left(e_s^{(k+1)} - e_w^{(k+1)}, \phi_s\right)_{sw} = 0 \end{cases} \tag{24}$$

Theorem 4.2 (Convergence of the iterative method)**.** *In the iterative method, the error functions are such that*

$$\lim_{k\to+\infty} (\|e_l^{(k)}\|_{1,l}^2 + \|e_w^{(k)}\|_{1,w}^2 + \|e_s^{(k)}\|_{1,s}^2) = 0.$$

Proof. By standard arguments (Cauchy-Schwarz and Young inequality), by taking $\phi_i = e_i^{(k+1)}$ (for $i = l, w, s$) in (24), we obtain the inequalities

$$\begin{cases} \hat{\alpha}_l\|e_l^{(k+1)}\|_{1,l}^2 + \frac{1}{2}\|e_l^{(k+1)}\|_{ls}^2 + \frac{1}{2}\|e_l^{(k+1)}\|_{lw}^2 \le \frac{1}{2}\|e_s^{(k)}\|_{ls}^2 + \frac{1}{2}\|e_w^{(k)}\|_{lw}^2 \\ \hat{\alpha}_w\|e_w^{(k+1)}\|_{1,w}^2 + \frac{1}{2}\|e_w^{(k+1)}\|_{lw}^2 + \frac{1}{2}\|e_w^{(k+1)}\|_{sw}^2 \le \frac{1}{2}\|e_s^{(k)}\|_{sw}^2 + \frac{1}{2}\|e_l^{(k+1)}\|_{lw}^2 \\ \hat{\alpha}_s\|e_s^{(k+1)}\|_{1,s}^2 + \frac{1}{2}\|e_s^{(k+1)}\|_{ls}^2 + \frac{1}{2}\|e_s^{(k+1)}\|_{sw}^2 \le \frac{1}{2}\|e_l^{(k+1)}\|_{ls}^2 + \frac{1}{2}\|e_w^{(k+1)}\|_{sw}^2 \end{cases} \tag{25}$$

Summing up the three equations in (25), we obtain

$$\hat{\alpha}_l\|e_l^{(k+1)}\|_{1,l}^2 + \hat{\alpha}_w\|e_w^{(k+1)}\|_{1,w}^2 + \hat{\alpha}_s\|e_s^{(k+1)}\|_{1,s}^2 + \frac{1}{2}\|e_s^{(k+1)}\|_{ls}^2 + \frac{1}{2}\|e_s^{(k+1)}\|_{sw}^2 + \frac{1}{2}\|e_w^{(k+1)}\|_{lw}^2 \le \frac{1}{2}\|e_s^{(k)}\|_{ls}^2 + \frac{1}{2}\|e_s^{(k)}\|_{sw}^2 + \frac{1}{2}\|e_w^{(k)}\|_{lw}^2.$$

Summing for $k = 0, \ldots, K-1$, we have

$$\min_{i=l,w,s}(\hat{\alpha}_i)\sum_{k=1}^{K}(\|e_l^{(k+1)}\|_{1,l}^2 + \|e_w^{(k+1)}\|_{1,w}^2 + \|e_s^{(k+1)}\|_{1,s}^2) \le \frac{1}{2}(\|e_s^{(0)}\|_{ls}^2 + \|e_s^{(0)}\|_{sw}^2 + \|e_w^{(0)}\|_{lw}^2).$$

Since the right-hand side is independent of K, we have that the sum of the series

$$\min_{i=l,w,s}(\hat{\alpha}_i)\sum_{k=1}^{\infty}(\|e_l^{(k+1)}\|_{1,w}^2 + \|e_w^{(k+1)}\|_{1,w}^2 + \|e_s^{(k+1)}\|_{1,s}^2)$$

is bounded, which implies the convergence. □

Remark 4.3. A similar proof is extended to the scheme with the sequence lumen-strut-wall.

4.2. **The "parallel" variant.** The previous iterative scheme uses the guess of the solution C_l, C_w, C_s as soon as it is available. For this reason, we will call it the "sequential" variant. A natural variant, oriented to parallel computation, reads as follows.

Let us assume that $C_l^{(0)}$, $C_w^{(0)}$ and $C_s^{(0)}$ are given (they may coincide with the converged value at the previous time step).

1. Lumen problem: Solve

$$\begin{aligned} &\chi C_l^{(k+1)} - \mu_l \Delta C_l^{(k+1)} + \boldsymbol{u} \cdot \nabla C_l^{(k+1)} = f_l && \text{in } \Omega_l \\ &\mu_l \frac{\partial C_l^{(k+1)}}{\partial \boldsymbol{n}_l} + \zeta_{ls}(C_l^{(k+1)} - C_s^{(k)}) = 0 && \text{on } \Gamma_{ls} \\ &\mu_l \frac{\partial C_l^{(k+1)}}{\partial \boldsymbol{n}_l} + \zeta_{lw}(C_l^{(k+1)} - C_w^{(k)}) = 0 && \text{on } \Gamma_{lw} \end{aligned}$$

   In weak terms: find $C_l^{(k+1)} \in V_l$ s.t.

$$\hat{a}_l(C_l^{(k+1)}, \phi_l) + \left(C_l^{(k+1)} - C_s^{(k)}, \phi_l\right)_{ls} + \left(C_l^{(k+1)} - C_w^{(k)}, \phi_l\right)_{lw} = (f_l, \phi_l)_l \quad (26)$$

   for all $\phi_l \in V_l$.
2. Wall problem: Solve

$$\begin{aligned} &\chi C_w^{(k+1)} - \mu_w \Delta C_w^{(k+1)} = f_w && \text{in } \Omega_w \\ &\mu_w \frac{\partial C_w^{(k+1)}}{\partial \boldsymbol{n}_w} + \zeta_{lw}(C_w^{(k+1)} - C_l^{(k)}) = 0 && \text{on } \Gamma_{lw} \\ &\mu_w \frac{\partial C_w^{(k+1)}}{\partial \boldsymbol{n}_w} + \zeta_{sw}(C_w^{(k+1)} - C_s^{(k)}) = 0 && \text{on } \Gamma_{sw} \end{aligned}$$

   In weak terms: find $C_w^{(k+1)} \in V_w$ s.t.

$$\hat{a}_w(C_w^{(k+1)}, \phi_w) + \left(C_w^{(k+1)} - C_l^{(k)}, \phi_w\right)_{lw} + \left(C_w^{(k+1)} - C_s^{(k)}, \phi_w\right)_{sw} = (f_w, \phi_w)_w \quad (27)$$

   for all $\phi_w \in V_w$.
3. Strut problem: Solve

$$\begin{aligned} &\chi C_s^{(k+1)} - \mu_s \Delta C_s^{(k+1)} = f_s && \text{in } \Omega_s \\ &\mu_s \frac{\partial C_s^{(k+1)}}{\partial \boldsymbol{n}_s} + \zeta_{ls}(C_s^{(k+1)} - C_l^{(k)}) = 0 && \text{on } \Gamma_{ls} \\ &\mu_s \frac{\partial C_s^{(k+1)}}{\partial \boldsymbol{n}_w} + \zeta_{sw}(C_s^{(k+1)} - C_w^{(k)}) = 0 && \text{on } \Gamma_{sw} \end{aligned}$$

   In weak terms: find $C_s^{(k+1)} \in V_s$ s.t.

$$\hat{a}_s(C_s^{(k+1)}, \phi_s) + \left(C_s^{(k+1)} - C_l^{(k)}, \phi_s\right)_{ls} + \left(C_s^{(k+1)} - C_w^{(k)}, \phi_s\right)_{sw} = (f_s, \phi_s)_s \quad (28)$$

   for all $\phi_s \in V_s$.
4. Relaxation: Set

$$C_{i,rel}^{(k+1)} = \omega_i C_i^{(k+1)} + (1 - \omega_i) C_i^{(k)}, i = l, w, s$$

where ω_i are real numbers generally in the interval $(0, 1]$. Again, for easiness of notation, we reset $C_i^{(k+1)} = C_{i,rel}^{(k+1)}$.

This approach is immediately parallelizable since the three problems (Lumen, Wall, Strut) can be solved simultaneously. Using again the notation introduced in (23), we have the following theorem.

Theorem 4.4 (Convergence of the parallel variant)**.** *The error functions of the parallel variant are such that*

$$\lim_{k\to+\infty} (\|e_l^{(k)}\|_{1,l}^2 + \|e_w^{(k)}\|_{1,w}^2 + \|e_s^{(k)}\|_{1,s}^2) = 0.$$

Proof. The proof is similar to the one for the sequential formulation. In this case, we have

$$\begin{cases} \hat{\alpha}_l \|e_l^{(k+1)}\|_{1,l}^2 + \frac{1}{2}\|e_l^{(k+1)}\|_{ls}^2 + \frac{1}{2}\|e_l^{(k+1)}\|_{lw}^2 \le \frac{1}{2}\|e_s^{(k)}\|_{ls}^2 + \frac{1}{2}\|e_w^{(k)}\|_{lw}^2 \\ \hat{\alpha}_w \|e_w^{(k+1)}\|_{1,w}^2 + \frac{1}{2}\|e_w^{(k+1)}\|_{lw}^2 + \frac{1}{2}\|e_w^{(k+1)}\|_{sw}^2 \le \frac{1}{2}\|e_s^{(k)}\|_{sw}^2 + \frac{1}{2}\|e_l^{(k)}\|_{lw}^2 \\ \hat{\alpha}_s \|e_s^{(k+1)}\|_{1,s}^2 + \frac{1}{2}\|e_s^{(k+1)}\|_{ls}^2 + \frac{1}{2}\|e_s^{(k+1)}\|_{sw}^2 \le \frac{1}{2}\|e_l^{(k)}\|_{ls}^2 + \frac{1}{2}\|e_w^{(k)}\|_{sw}^2 \end{cases} \tag{29}$$

leading to

$$\begin{aligned} &\hat{\alpha}_l \|e_l^{(k+1)}\|_{1,l}^2 + \hat{\alpha}_w \|e_w^{(k+1)}\|_{1,w}^2 + \hat{\alpha}_s \|e_s^{(k+1)}\|_{1,s}^2 + \frac{1}{2}\|e_s^{(k+1)}\|_{ls}^2 + \\ &\quad \frac{1}{2}\|e_s^{(k+1)}\|_{sw}^2 + \frac{1}{2}\|e_w^{(k+1)}\|_{sw}^2 + \frac{1}{2}\|e_w^{(k+1)}\|_{lw}^2 + \frac{1}{2}\|e_l^{(k+1)}\|_{ls}^2 + \frac{1}{2}\|e_l^{(k+1)}\|_{lw}^2 \\ &\quad \le \frac{1}{2}\|e_s^{(k)}\|_{ls}^2 + \frac{1}{2}\|e_s^{(k)}\|_{sw}^2 + \frac{1}{2}\|e_w^{(k)}\|_{sw}^2 + \frac{1}{2}\|e_w^{(k)}\|_{lw}^2 + \frac{1}{2}\|e_l^{(k)}\|_{ls}^2 + \frac{1}{2}\|e_l^{(k)}\|_{lw}^2. \end{aligned}$$

Summing up for $k = 0, \dots, K-1$, we have

$$\begin{aligned} &\min_{i=l,w,s} (\hat{\alpha}_i) \sum_{k=1}^{K} (\|e_l^{(k+1)}\|_{1,l}^2 + \|e_w^{(k+1)}\|_{1,w}^2 + \|e_s^{(k+1)}\|_{1,s}^2) \\ &\le \frac{1}{2}(\|e_s^{(0)}\|_{ls}^2 + \|e_s^{(0)}\|_{sw}^2 + \|e_w^{(0)}\|_{sw}^2 + \|e_w^{(0)}\|_{lw}^2 + \|e_l^{(0)}\|_{lw}^2 + \|e_l^{(0)}\|_{ls}^2). \end{aligned}$$

Since the right-hand side is independent of K, we obtain the thesis for $K \to +\infty$. □

5. **Numerical results.** We start considering a simplified geometrical setting like the one in Fig. 3 (right). The struts form a sequence of rings centered on the centerline of the pipe. We consider sequences of 1, 3, and 5 rings on both a straight and a curved pipe. The pipe is 5 mm long, with an external radius of 1.2 mm (external wall); the wall-lumen interface is located at the radius $R_l = 1$ mm. The internal face of the struts (interfacing with the lumen) is at a distance of 0.9 mm from the centerline, the external face (interfacing with the wall) is at 1.08 mm, and the length of each ring is 0.2 mm.

We implemented our domain decomposition method within the NGSolve library [25], through Python scripts. The meshes were generated with the companion mesh generator NetGen.

We wrote a simple unsteady Navier-Stokes solver for the flow in the lumen. The boundary conditions for the Navier-Stokes problem were set to be:

1. no-slip (i.e., homogeneous Dirichlet) at the interface of the lumen with either the wall or the struts;
2. non-homogeneous Dirichlet at the inflow with a Poiseuille flow at the inflow circular section;

3. traction-free (i.e., homogeneous Neumann) at the outflow.

At this proof-of-concept stage, we tested different diffusivities. In particular, when in Ω_l the convection is dominating over the diffusion we stabilized the solver with a strongly consistent method like SUPG [3]. In the following results, we set the diffusivities to be $\mu_l = 5.0 \times 10^{-5}$, $\mu_w = 5.0 \times 10^{-5}$, $\mu_s = 1.0 \times 10^{-9}$ mm^2/s respectively. The Robin constants ζ_{lw} and ζ_{ls}, in general, are functions of the shear stress $\nu(\nabla \boldsymbol{u} + \nabla^T \boldsymbol{u}) \cdot \boldsymbol{n} - \boldsymbol{n} \cdot \big(\nu(\nabla \boldsymbol{u} + \nabla^T \boldsymbol{u}) \cdot \boldsymbol{n}\big)\boldsymbol{n}$. For the sake of simplicity, we assume here these coefficients to be constant: $\zeta_{lw} = 3.42 \times 10^{-3}$, $\zeta_{ls} = 3.42 \times 10^{-3}$, and $\zeta_{sw} = 3.5 \times 10^{-3}$ mm/s respectively.

In this first round of simulations, we set the initial conditions to be $C_{l,0} = 1$, $C_{w,0} = 0.5$ and $C_{s,0} = 0$, to mimic the evolution of blood solutes (similar to the case considered in [22, 23] with only two subdomains, lumen and wall).

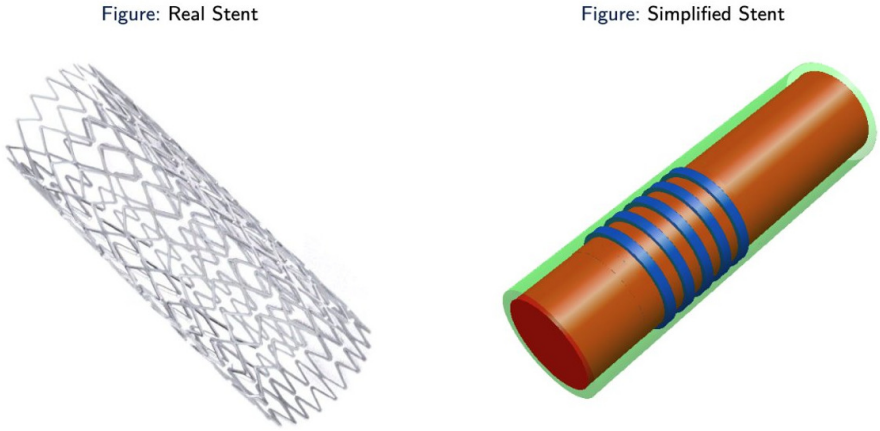

FIGURE 3. Left: Real-life stent. Right: Simplified stent with five rings.

We focus only on the sequential variant of the domain-decomposition method, as this will be the subject of our subsequent analysis. The convergence of the parallel variant was confirmed by numerical results too.

The results are reported in Fig. 4, 5, 6, 7, 8, 9.

The quantitative assessment is reported in Tab. 1. We report the number of iterations and the CPU time. Similar results were obtained also in the case of curved pipes.

2-Rings			3-Rings			5-Rings		
# El	# It	Time [s]	# El	# It	Time [s]	# El	# It	Time [s]
2000	4	1.64	3418	4	2.86	4107	4	3.74
6073	4	4.90	6596	5	6.40	7527	5	6.84
25256	5	27.25	26333	5	30.23	27157	5	30.60
48584	4	45.31	52768	4	47.31	60216	4	56.19
128000	4	213.27	142272	4	252.13	175424	4	324.16

TABLE 1. Numerical results for different numbers of stent rings and mesh elements.

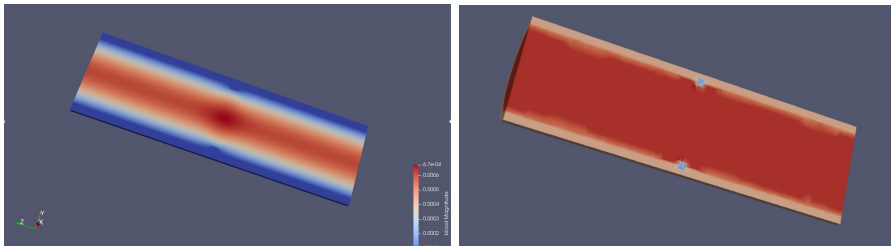

FIGURE 4. Left: Blood velocity with one-ring stent. Right: Solute with one-ring stent

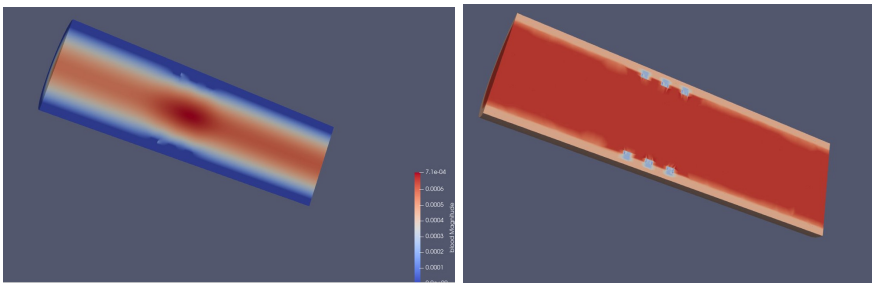

FIGURE 5. Left: Blood velocity with the three-ring stent. Right: Solute with three-ring stent

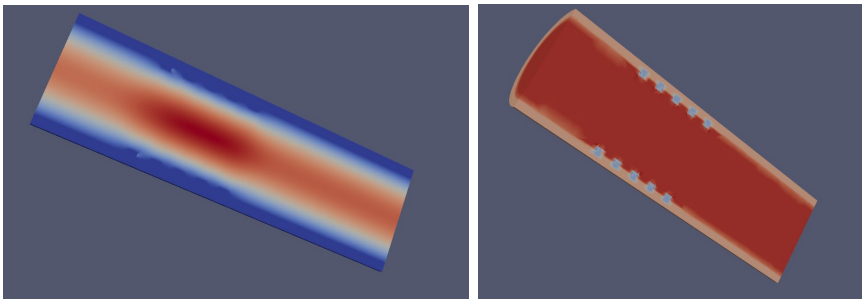

FIGURE 6. Left: Blood velocity with the five-ring stent. Right: Solute with five-ring stent

5.1. **Sensitivity on the diffusivity.** We performed additional simulations by changing the diffusivity parameters in the lumen, wall, and stent to probe further our domain decomposition method under different conditions. We first consider the following cases: $\mu_w = 1.0 \times 10^{-3}$, $\mu_l = 1.0 \times 10^{-5}$, $\mu_s = 1.0 \times 10^{-9}$ mm^2/s (negligible diffusivity in the stent, like for Bare Metallic Stents); $\mu_w = 1.0 \times 10^{-3}$, $\mu_l = 1.0 \times 10^{-5}$, $\mu_s = 1.0 \times 10^{-7}$ mm^2/s (low diffusive stent); and $\mu_w = 1.0 \times 10^{-3}$, $\mu_l = 1.0 \times 10^{-5}$, $\mu_s = 1.0 \times 10^{-1}$ mm^2/s (high diffusive stent). SUPG stabilization was introduced in the lumen problem to manage the convective-dominated nature of the problem.

The results are reported in Figures 10 and 11. There is a noticeable difference in the absorption from lumen to wall while only a small discrepancy can be observed from their respective interactions with the stent. When it comes to low diffusivity

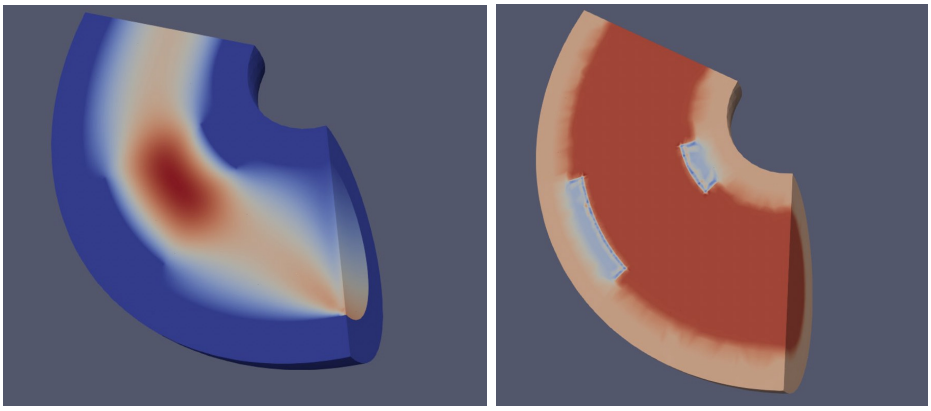

FIGURE 7. Left: Blood velocity with one-ring curved stent. Right: Solute with one-ring curved stent

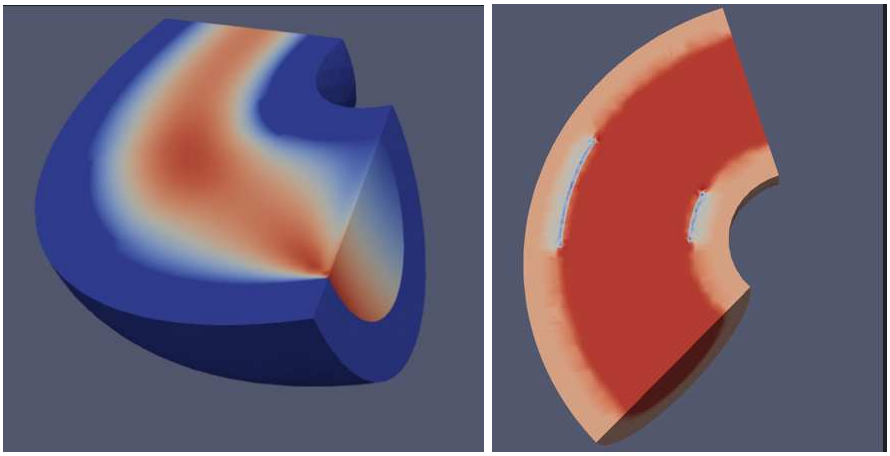

FIGURE 8. Left: Blood velocity with one-ring curved thin stent. Right: Solute with one-ring curved thin stent.

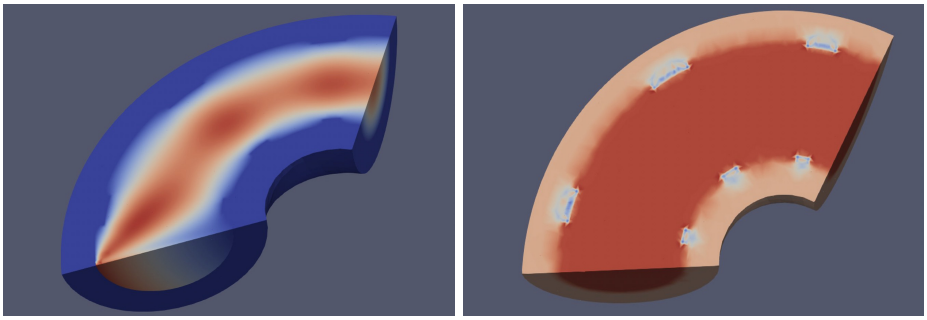

FIGURE 9. Left: Blood velocity with three-ring curved stent. Right: Solute with three-ring curved thin stent.

in the stent, the concentration shifts more around the stent; and for high diffusivity in the stent, more variability in all regions around the struts can be appreciated. When the struts had higher diffusivity, the maximum concentration decreases, and vice versa. This is due the fact that the concentration is spread across more regions instead of gathering in fewer areas.

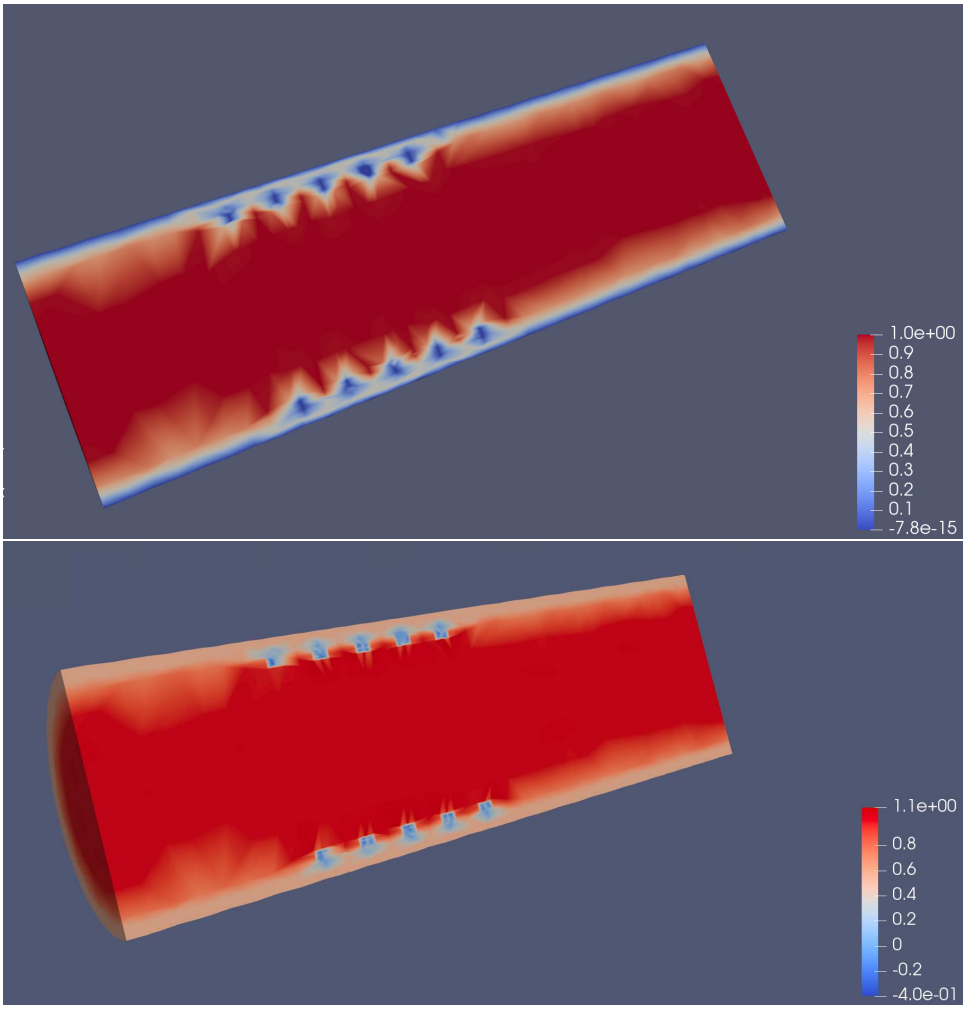

FIGURE 10. Solute concentration in five-ring stent with different diffusivity in the wall and the lumen after one iteration (top), and after five iterations (bottom).

5.2. **More involved and realistic stents design.** We now present two cases with more realistic geometries. The first consists of a stent that has been designed like a net, as can be observed in Figure 12.

The lumen and artery wall diameters are 4 mm and 5 mm, respectively, and 8 mm in length. The thickness of the stent is 0.2 mm, and the mesh as a whole contains 64812 elements. After implementing parameters $\mu_w = 1.0 \times 10^{-3}$, $\mu_l = 1.0 \times 10^{-5}$, $\mu_s = 1.0 \times 10^{-9}$ in the multidomain simulations, the blood and solute behavior are

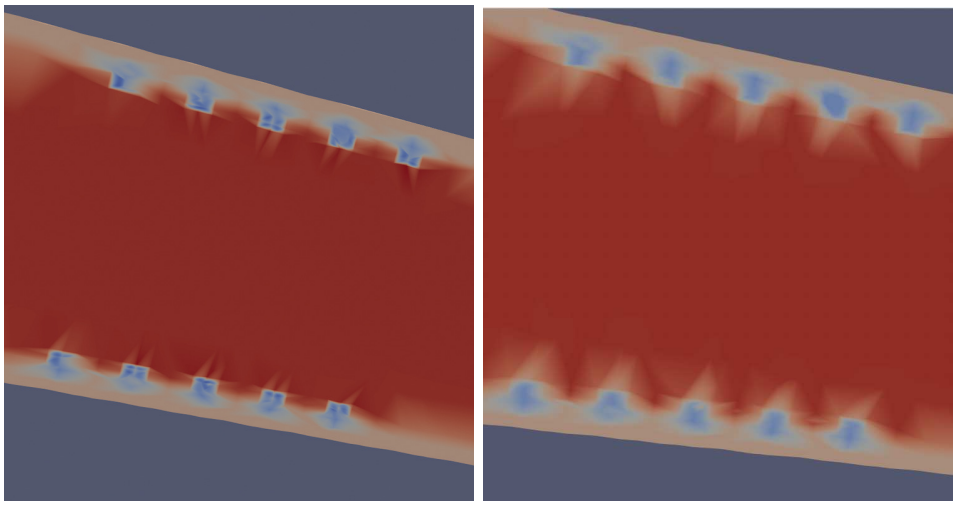

FIGURE 11. Left: Solute concentration in five-ring stent with low diffusivity in the struts. Right: Solute concentration in five-ring stent with high diffusivity in the struts

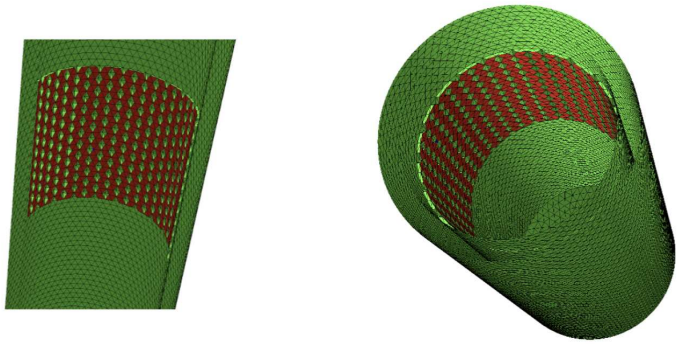

FIGURE 12. Net-like stent

reflected in Figure 13. It can be readily seen that this particular geometry increases the perturbation of the flow and acts as a local blockage for solutes.

The design of the stent incorporated in the second result is inspired by a real Xience Prime stent see [6].

For our mesh, we kept the same size as in the previous instance with the exception of the strut thickness, which is now 80 microns for realistic purposes. The mesh in Figure 14 has 115899 elements

We highlight the results of the multidomain simulations in Figure 15.

This time the blood flow is slightly perturbed by the presence of the stent, due to the decreased thickness of the stent, while a more oscillatory solute movement can be captured in the endothelial layer (i.e. the interface Γ_{lw}). The domain decomposition method converges and the results meet the expectation of the geometrical influence of the stent on the blood velocity and transfer of solutes to the artery wall. Also in

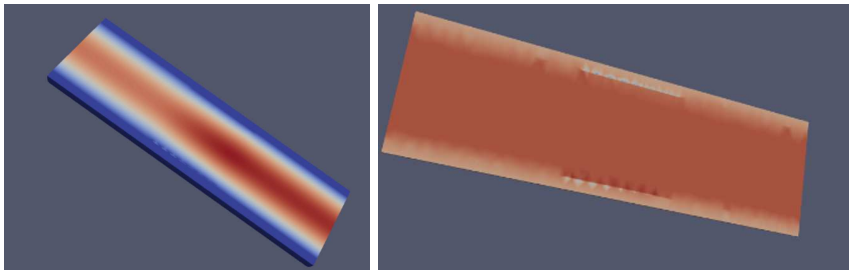

FIGURE 13. Left: Blood behavior under a net-like stent. Right: Solute behavior in the presence of the same stent.

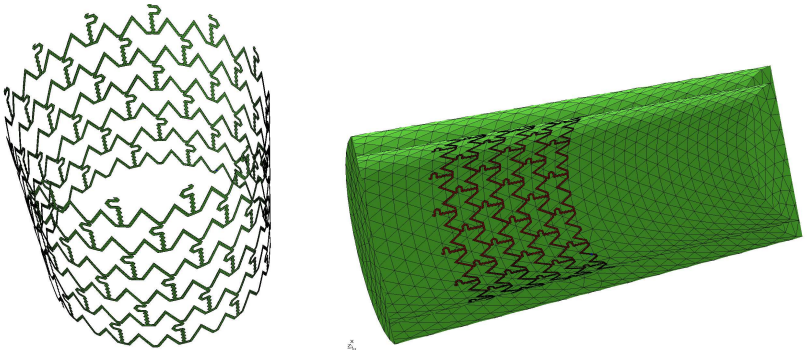

FIGURE 14. Mesh of stent designed upon a real device [6].

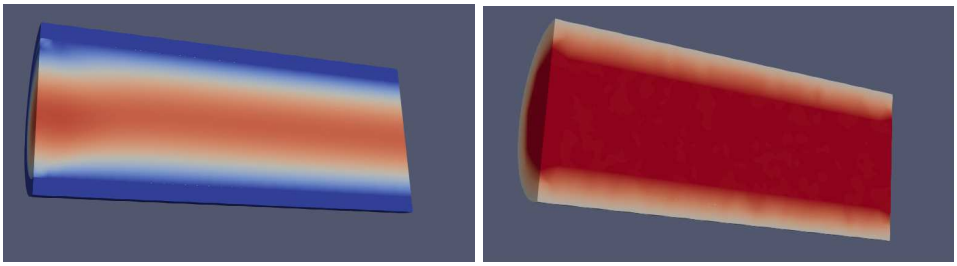

FIGURE 15. Left: Blood simulation of realistic stent. Right: Solute behavior of realistic stent.

this case, the number of iterations of the domain-decomposition scheme turned out to be independent of the mesh size.

5.3. **Drug elution setup in DES/BRS.** Setting $C_{w,0}$, $C_{l,0}$ to be zero with $C_{s,0} = 1$ and a relatively higher diffusivity μ_s, we mimic the case of DES/BRS. In Figure 16, we can observe that, with these settings, drug elutes from the strut to the wall and the lumen as expected.

5.4. **Independence of the convergence rate of the mesh size.** The numerical results presented here not only confirm the convergence Theorem but demonstrate that the convergence rate of the method is independent of the mesh size, so we can say that it is "optimal." This is a critical feature in view of realistic applications of

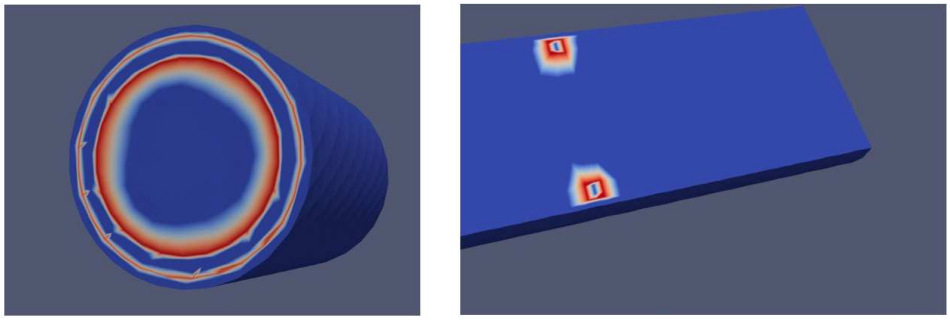

FIGURE 16. Cross-sections of drug-eluting stents when $C_s(t = 0) = 1$, $C_l(t = 0) = 0$, $C_w(t = 0) = 0$: the drug is released from the struts to the other domains.

the method, as it guarantees that the cost of cases requiring fine meshes will depend mainly on the cost of each iteration. Optimality of a similar domain-decomposition method with only two domains (lumen and wall) was proven in [22, 23] resorting to Steklov-Poincaré (SP) operators [20]. This means that the original problem was reformulated as an interface functional equation. Successively, the domain-decomposition method was reinterpreted as a preconditioned Richardson scheme. The preconditioner was identified as one of the SP operators with features that - in view of available results for preconditioned Richardson method and the so-called Finite Element Uniform Extension Theorem - allow a conclusion for the optimality. The extension of this reinterpretation to this problem is not trivial at all. As a matter of fact, we have three interfaces here, so the SP reinterpretation leads to a system of functional equations, and the interpretation of the domain-decomposition method as a preconditioned Richardson scheme is not immediate. We will investigate this approach in a forthcoming paper to prove rigorously the mesh-independence.

6. **Conclusions.** In this paper, we consider for the first time the elution in a stented artery when all the subdomains are in contact, as it happens in real cases. An accurate and efficient modeling of this problem is critical for the optimized design of next-generation stents. The analysis of the multiphysics problem, even for a simplified elution process, raises some challenges. While our numerical evidence displays a substantial optimal behavior of our domain decomposition scheme with respect to the mesh size, the actual rigorous proof of this is not trivial and will be subject of additional investigations.

Beyond the theoretical work, in the next steps of the present research, we intend to (i) apply our segregated method to real geometries reconstructed from the literature [14]; (ii) improve the accuracy of the elution model, with a multiphase model for the strut elution [7]; (iii) model the erosion over a larger time scale, so to include the geometrical changes of the subdomains in time and, possibly, to predict the erosion patterns on the struts.

This is the first step toward a mathematically-oriented design of bioresorbable prostheses, that may avoid the failures of the previous scaffolds.

Data availability statement. The present work does not involve any human data and does not need any IRB approval. The datasets generated during and/or analyzed during the current study are available from the corresponding author upon reasonable request.

Acknowledgments. The authors wish to thank the team of people working on stents from the biomedical point of view who inspired this work: Habib Samady, David Molony (North Georgia Healthcare System, Gainsville, GA USA), Adrien Lefieux (INRIA, Paris, FR), and Imran Shah (GA Tech & Emory University, Atlanta, GA USA). They also want to acknowledge the outstanding contribution of the anonymous Referees in improving and making rigorous the analysis of the domain-decomposition scheme.

REFERENCES

[1] H. Brezis, *Functional Analysis, Sobolev Spaces, and Partial Differential Equations*, Springer, 2011.
[2] F. Brezzi and G. Gilardi, Chapters 1-3 in *Finite Element Handbook*, H. Kardestuncer and D.H. Norrie, McGraw-Hill Book Co., New York, 1987.
[3] A. N. Brooks and T. J. R. Hughes, Streamline Upwind/Petrov-Galerkin formulations for convection dominated flows with particular emphasis on the incompressible Navier-Stokes equations, *Computer Methods in Applied Mechanics and Engineering*, **32** (1982), 199-259.
[4] D. Capodanno, Bioresorbable scaffolds in coronary intervention: Unmet needs and evolution, *Korean Circulation Journal*, **48** (2018), 24-35.
[5] Mayo Clinic, Coronary angioplasty and stents, `https://www.mayoclinic.org/tests-procedures/coronary-angioplasty/about/pac-20384761`
[6] N. Foin, S. Sen, E. Allegria, R. Petraco, S. Nijjer, D. Francis, C. Di Mario and J. Davies, Maximal expansion capacity with current DES platforms: A critical factor for stent selection in the treatment of left main bifurcations, *EuroIntervention*, **8** (2013), 1315-1325.
[7] L. Formaggia, S. Minisini and P. Zunino, Modeling polymeric controlled drug release and transport phenomena in the arterial tissue, *Mathematical Models and Methods in Applied Sciences*, **20** (2010), 1759-1786.
[8] F. Giannini, L. Candilio, S. Mitomo, N. Ruparelia, A. Chieffo, L. Baldetti, F. Ponticelli, A. Latib and A. Colombo, A practical approach to the management of complications during percutaneous coronary intervention, *JACC: Cardiovascular Interventions*, **11** (2018), 1797-1810.
[9] J. Heywood, The Navier-Stokes equations: On the existence, regularity and decay of solutions, *Indiana Univ. Math. J.*, **29** (1980), 639-681.
[10] J. Heywood and R. Rannacher, Finite element approximation of the nonstationary Navier-Stokes Problem. i. Regularity of solutions and second-order error estimates for spatial discretization, *SIAM J. Numer. Anal.*, **19** (1982), 275-311.
[11] E. Hopf, Uber die aufgangswertaufgabe fur die hydrodynamischen grundliechungen, *Math. Nachr.*, **4** (1951), 213-231.
[12] H. Jinnouchi, S. Torii, A. Sakamoto, F. D. Kolodgie, R. Virmani and A. V. Finn, Fully bioresorbable vascular scaffolds: Lessons learned and future directions, *Nature Reviews Cardiology*, **16** (2019), 286-304.
[13] K. C. Koskinas, Y. S. Chatzizisis, A. P. Antoniadis and G. D. Giannoglou, Role of endothelial shear stress in stent restenosis and thrombosis: Pathophysiologic mechanisms and implications for clinical translation, *Journal Of The American College Of Cardiology*, **59** (2012), 1337-1349.
[14] A. Lefieux, S. Bridio, D. Molony, M. Piccinelli, C. Chiastra, H. Samady, F. Migliavacca and A. Veneziani, Semi-automatic reconstruction of patient-specific stented coronaries based on data assimilation and computer aided design, *Cardiovascular Engineering and Technology*, **13** (2022), 517-534.
[15] J. Leray, Etude de diverses èquations intègrales et de quelques problèmes que pose l'hydrodynamique, *J. Math. Pures Appl.*, **12** (1933), 1-82.

[16] J. Leray, Sur les mouvement d'un liquide visqueux emplissant l'espace, *Acta. Math.*, **63** (1934), 193-248.
[17] J. Leray, Essai sur les mouvements plans d'un liquide visqueux que limitent des parois, *J. Math. Pures Appl.*, **13** (1934), 331-418.
[18] Y. Onuma and P. Serruys, *Bioresorbable Scaffolds: From Basic Concept to Clinical Applications*, CRC Press, 2017.
[19] R. Piccolo, A. Franzone and S. Windecker, From bare metal to barely anything: An update on coronary stenting, *Heart*, **104** (2018), 533-540.
[20] A. Quarteroni and A. Valli, *Domain Decomposition Methods for Partial Differential Equations*, Oxford University Press, 1999.
[21] A. Quarteroni and A. Valli, *Numerical Approximation of Partial Differential Equations*, Springer Science & Business Media, 2008.
[22] A. Quarteroni, A. Veneziani and P. Zunino, A domain decomposition method for advection-diffusion processes with application to blood solutes, *SIAM Journal on Scientific Computing*, **23** (2002), 1959-1980.
[23] A. Quarteroni, A. Veneziani and P. Zunino, Mathematical and numerical modeling of solute dynamics in blood flow and arterial walls, *SIAM Journal on Numerical Analysis*, **39** (2002), 1488-1511.
[24] A. Quarteroni, M. Tuveri and A. Veneziani Computational vascular fluid dynamics: Problems, models and methods, *Comput. Visual. Sci.*, **2** (2000), 163-197.
[25] J. Schroebel, Netgen/NGSolve, `https://ngsolve.org/`.
[26] R. Temam, *Navier-Stokes Equations and Nonlinear Functional Analysis*, SIAM, 1983.
[27] R. Temam, *Navier-Stokes Equations: Theory and Numerical Analysis*, North-Holland, 1984.
[28] M. Zilberman and R. C. Eberhart, Drug-eluting bioresorbable stents for various applications, *Annual Review of Biomedical Engineering*, **8** (2006), 153-180.

Received November 2023; 1st revision December 2023; 2nd revision April 2024; early access June 2024.